Epilepsy Research 159 (2020) 106244

Contents lists available at ScienceDirect

Epilepsy Research

journal homepage: www.elsevier.com/locate/epilepsyres

Modulation of epileptogenesis: A paradigm for the integration of enzyme-based microelectrode arrays and optogenetics

Corwin R. Butler[a,1], Jeffery A. Boychuk[a,b,1], Francois Pomerleau[d,h], Ramona Alcala[e], Peter Huettl[d,h], Yi Ai[d], Johan Jakobsson[i], Sidney W. Whiteheart[f,g], Greg A. Gerhardt[b,c,d,e,h], Bret N. Smith[a,b,c,d], John T. Slevin[b,e,g,h,*]

[a] Department of Physiology, College of Medicine, University of Kentucky, Lexington, KY, 40536, United States
[b] Epilepsy Center, University of Kentucky, Lexington, KY, 40536, United States
[c] Spinal Cord and Brain Injury Research Center (SCoBIRC), University of Kentucky, Lexington, KY, 40536, United States
[d] Department of Neuroscience, College of Medicine, University of Kentucky, Lexington, KY, 40536, United States
[e] Department of Neurology, College of Medicine, University of Kentucky, Lexington, KY, 40536, United States
[f] Department of Molecular and Cellular Biochemistry, University of Kentucky, Lexington, KY, 40536, United States
[g] Veterans Affairs Medical Center, Lexington, KY, 40536, United States
[h] Brain Restoration Center, University of Kentucky, Lexington, KY, 40356, United States
[i] Wallenburg Neuroscience Center, Lund Stem Cell Center, Lund University, Lund, Sweden

ARTICLE INFO

Keywords:
Dentate gyrus
Epileptogenesis
Glutamate
Microelectrode array
Optogenetics

ABSTRACT

Background: Genesis of acquired epilepsy includes transformations spanning genetic-to- network-level modifications, disrupting the regional excitatory/inhibitory balance. Methodology concurrently tracking changes at multiple levels is lacking. Here, viral vectors are used to differentially express two opsin proteins in neuronal populations within dentate gyrus (DG) of hippocampus. When activated, these opsins induced excitatory or inhibitory neural output that differentially affected neural networks and epileptogenesis. In vivo measures included behavioral observation coupled to real-time measures of regional glutamate flux using ceramic-based amperometric microelectrode arrays (MEAs).

Results: Using MEA technology, phasic increases of extracellular glutamate were recorded immediately upon application of blue light/488 nm to DG of rats previously transfected with an AAV 2/5 vector containing an (excitatory) channelrhodopsin-2 transcript. Rats receiving twice-daily 30-sec light stimulation to DG ipsilateral to viral transfection progressed through Racine seizure stages. AAV 2/5 (inhibitory) halorhodopsin-transfected rats receiving concomitant amygdalar kindling and DG light stimuli were kindled significantly more slowly than non-stimulated controls. In in vitro slice preparations, both excitatory and inhibitory responses were independently evoked in dentate granule cells during appropriate light stimulation. Latency to response and sensitivity of responses suggest a degree of neuron subtype-selective functional expression of the transcripts.

Conclusions: This study demonstrates the potential for coupling MEA technology and optogenetics for real-time neurotransmitter release measures and modification of seizure susceptibility in animal models of epileptogenesis. This microelectrode/optogenetic technology could prove useful for characterization of network and system level dysfunction in diseases involving imbalanced excitatory/inhibitory control of neuron populations and guide development of future treatment strategies.

1. Introduction

The precise mechanisms that drive epileptogenesis are unknown. Clearly, there are many potential triggering events. Changes occur over time at many levels of organization, including genetic alterations, molecular and biochemical modifications, alterations of channels and neurotransmission, morphologic and cellular reorganization, and network transformations (Klein et al., 2018). Which of these processes is

* Corresponding author at: Kentucky Clinic J-401, University of Kentucky College of Medicine, 740 South Limestone Street, Lexington, KY, 40536-0284, United States.
E-mail address: jslevin@uky.edu (J.T. Slevin).
[1] Authors contributed equally.

https://doi.org/10.1016/j.eplepsyres.2019.106244
Received 21 September 2019; Received in revised form 22 October 2019; Accepted 22 November 2019
Available online 26 November 2019
0920-1211/

transcendent and whether any singular modification represents a common node for the multiple causations ultimately leading to the behavioral expression of spontaneous seizures is unknown. Regardless, acquired epilepsy, the product of the process of epileptogenesis, is associated with increased likelihood of pathological hyper-synchronous activation of large populations of neurons that may occur through imbalanced secretion of both excitatory (glutamate) and inhibitory (GABA) neurotransmitters. Understanding the contribution of cellular excitability to the process of epileptogenesis will be critical for developing disease-modifying therapies to prevent the development of acquired epilepsy.

Specific, targeted control of neural systems to establish causality between neuronal activity and behavior has remained difficult to achieve until recent technological advances, including optogenetics, which introduces light sensitive proteins (opsins) into neurons that regulate transmembrane ion conductance (Boyden et al., 2005; Deisseroth et al., 2015). The most common opsins in use modulate membrane potentials, including blue light (488 nm)-activated channelrhodopsin (ChR2, excitation) and yellow light (593 nm)-activated halorhodopsin (NpHR, hyperpolarization) (Govorunova et al., 2015; Nagel et al., 2003). Most studies to date have reported the ability of opsin transfection to modify behavior and *ex vivo* synaptic function and some have investigated targeting of different opsin promoters to differing neuron subpopulations (Khoshkhoo et al., 2017). Here, amperometric glutamate microelectrode recordings, immunolabeling, whole cell patch-clamp electrophysiology, and behavioral responses to electrical kindling were used to investigate targeting of different opsins to glutamatergic and GABAergic neuronal populations within the hippocampus, using a single adenoviral serotype. This multipronged, temporal approach allows network, neuronal, and presynaptic release changes to be linked to biochemical, anatomical, electrophysiological, and behavioral outcomes associated with epileptogenesis. The functional and behavioral outcomes of transfecting these opsins is discussed.

2. Materials and methods

2.1. Viral construct and hippocampal viral injections

The viral vectors used in this study were pseudotyped AAV2/5 vectors, where the transgene of interest is flanked by inverted terminal repeats of the AAV2 packaged in an AAV5 capsid. The AAV vectors were produced using a double-transfection method with the plasmid (pAAV-hSyn-hChR2(H134R)-EYFP or pAAV-hSyn-NpHR3.0-EYFP) and the appropriate helper plasmid containing the essential adenoviral packaging genes, as previously described (Ulusoy et al., 2009). The final titers of the injected AAV vector suspensions were between 2.4e +14 and 2.8e+14 genome copies/mL.

All animal procedures were approved by the University of Kentucky Institutional Animal Care and Use Committee. Male Sprague-Dawley rats (Harlan Laboratories, Indianapolis, IN, U.S.A.) were used for these experiments. At 18–24 weeks of age, rats were anesthetized with isoflurane (1–3 %) and placed in a stereotaxic frame. A midline incision was made on the scalp to expose the skull. A burr hole was made above the dentate gyrus (DG) of the hippocampus (from bregma: AP: -4.4 mm; ML: -2.2 mm; Paxinos and Watson, 2005). A Hamilton syringe was loaded with 1 µL of the channelrhodopsin (488 nm; blue light activation; pAAV-hSyn-hChR2(H134R)-EYFP) or halorhodopsin (593 nm; yellow light activation; pAAV-hSyn-NpHR3.0-EYFP) suspension (in PBS) and was lowered to the DG (DV: -4.0) where the suspension was slowly injected over 4 min. The tissue was allowed to rest for 5 min before the needle was slowly retracted. Five to 7 weeks was allowed before experimentation was started to allow for near maximal expression of the vector to occur (Zhang et al., 2010).

2.2. In vivo amperometric measures of glutamate using microelectrode assemblies (MEAs)

Amperometric recordings, (100 kHz data acquisition displayed at a display frequency of 10 Hz), were performed using the FAST16mkIII recording system (Fast Analytical Sensing Technology, Quanteon, LLC, Nicholasville, KY). Ceramic-based Microelectrode arrays (MEAs) consisting of four platinum (Pt) recording sites measuring 15 × 333 µm arranged vertically in dual pairs (S2 conformation) were configured to measure glutamate as previously described (Burmeister et al., 2013). Briefly, a solution of 1 % Glutamate-oxidase (GluOx; US Biological, Salem, MA), 1 % bovine serum albumin (BSA; Sigma-Aldrich, St. Louis, MO) and 0.125 % glutaraldehyde (Glut; Sigma-Aldrich), was prepared and coated onto the bottom pair of recording sites to allow for the conversion of glutamate to α-ketoglutarate and the reporter molecule, H_2O_2, which can be oxidized at the surface of the Pt with an applied potential of +0.7 V vs Ag/AgCl. The top pair of recording sites, or the sentinel sites, only received a coating of the BSA/Glut matrix. This coating configuration allows for background measures and subtraction to obtain a self-referenced glutamate signal for measures of both tonic and phasic glutamate (Burmeister et al., 2013; Burmeister and Gerhardt, 2001). To make the electrode even more specific for glutamate and to eliminate electroactive interfering molecules such as ascorbic acid and dopamine from reaching the Pt sites, 1,3-phenylenediamine (mPD), a molecular size exclusion layer, was electroplated onto all 4 Pt recording sites (Burmeister et al., 2013). Before in vivo use, an in vitro calibration was used to determine selectivity (glutamate vs. ascorbic acid), sensitivity (slope, in nAmps/µM), and limit of detection (in µM based on a signal-to-noise ratio of 3), as previously described (Burmeister et al., 2013).

2.3. MEA and optical fiber configuration

For this study, the transfected channelrhodopsin (ChR2) was stimulated locally by affixing a guide cannula (Plastics One Roanoke VA) to the MEA. A fiber optic cannula (Ø200 µm Core, 0.39 NA; Thorlabs, Newton, NJ) was then inserted through the guide with the tip of the fiber positioned ~ 200 µm from the surface of the MEA in between all 4 Pt sites (see Fig. 1). The laser source (OBIS LS 488 nm, 100 mW, Coherent, Santa Clara, CA) was controlled through its analog port using a Master-8 pulse generator (A.M.P.I., Jerusalem, Israel). Pulse trains (100 pulses, 40 Hz) with variable pulse durations (1 − 20 ms) generating light intensities between 1–20 mW or constant light stimulation of variable intensities (1 − 50 mW) was delivered locally through the fiber optic cannula.

2.4. Electrical kindling

Fourteen-week-old male Sprague-Dawley rats (Harlan Laboratories) had stimulating electrodes surgically implanted in the right amygdala [from bregma: AP, 2.8; ML, +4.8; DV, 8.5; nose bar, 3.3 (flat skull)] as previously described (Matveeva et al., 2007). Animals were each tested for their after discharge (AD) threshold prior to kindling. An S88 dual channel stimulator (Grass Technologies, West Warwick, RI, U.S.A.) delivered a 1 s train of biphasic square wave pulses (1 ms pulse duration, 60 Hz) starting at an initial 100 µA until an AD was recorded on electroencephalography (EEG); this AD threshold was used for subsequent stimulation. About one third of animals exhibited no behavioral activity, and two-thirds experienced facial clonus (stage 1) or head nodding (stage 2) at their established AD threshold. Animals were housed individually in an enriched environment and maintained on a 12 h light/dark cycle with food and water available ad libitum. For amygdala kindling, rats that had received an injection of NpHR were also affixed with a waveguide cannula (Ø200 µm Core, 0.39 NA; Thorlabs, Newton, NJ) targeted in the DG and received a light stimulation (~ 2 − 3 sec duration; 593 nm; ~50 mW; LaserGlow

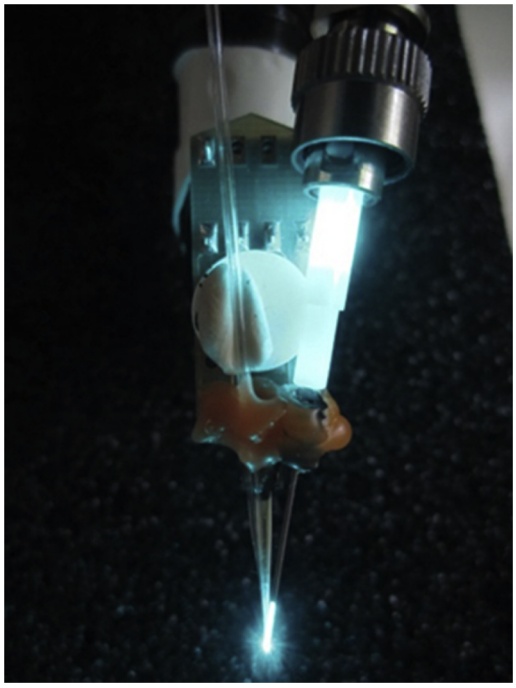

Fig. 1. MEA with attached fiber optic cannula and glass pipette.

technologies) immediately before the start of the kindling stimulus (1 s).

ChR2 "kindling": Some ChR2 injected animals were implanted with a waveguide cannula (Ø200 µm Core, 0.39 NA; Thorlabs, Newton, NJ) targeted to the DG. Animals were stimulated (30 s) with a blue light laser at 50 mW power (OBIS LS 488 nm, Coherent, Santa Clara, CA). Unless specifically stated, all animals were stimulated twice daily, 5 days per week, until they experienced two consecutive Racine stage 5 seizures (tonic–clonic activity with loss of postural control/falling (Racine, 1972)).

2.5. Slice preparation

Slices used for electrophysiological studies were obtained from rats 6 weeks after viral inoculation (i.e., 24–30 weeks of age). Rats were deeply anesthetized by isoflurane inhalation (5 %) and decapitated while anesthetized. The brain was removed and placed in ice-cold (2 − 4 °C) oxygenated artificial cerebrospinal fluid (ACSF) containing, in mM: 124 NaCl, 3 KCl, 2 $CaCl_2$, 26 $NaHCO_3$, 1.3 $MgCl_2$, 11 glucose and 1.4 NaH_2PO_4 equilibrated with bubbling 95 % O_2-5 % CO_2 (pH 7.2–7.4). Brains were blocked and glued to a sectioning stage, and 350 µm-thick slices were cut in the coronal plane in cold, oxygenated ACSF using a vibrating microtome (Vibratome Series 1000; Technical Products International, St. Louis, MO). Slices were transferred to a chamber containing oxygenated ACSF at 32 − 34 °C, where they were equilibrated for at least one hour prior to recording. Slices of the septal hippocampus were used in these experiments from viral injected rats and comparable slices from saline injected rats.

2.6. Whole cell recordings

Coronal hippocampal slices containing the dorsal third of the dentate gyrus were transferred to a recording chamber on an upright, fixed-stage microscope equipped with infrared, differential interference contrast optics (i.e., IR-DIC; Olympus BX50WI), where they were perfused with continuously warmed (32 − 34 °C) ACSF. Recordings were performed from dentate granule cells as described previously (Boychuk et al., 2016; Butler et al., 2015, 2016; Butler et al., 2017). Recording pipettes were pulled from borosilicate glass (1.65 mm outer diameter, 0.45 mm inner diameter; King Precision Glass, Claremont, CA) with a P-87 puller (Sutter Instrument, Novato, CA). The intracellular solution contained (in mM): 130 K^+-gluconate, 1 NaCl, 5 EGTA, 10 HEPES, 1 $MgCl_2$, 1 $CaCl_2$, 3 KOH, and 2 ATP. Open tip series resistance was 2–5 MOhms. Recordings were obtained using an Axon 700B amplifier (Molecular Devices), low-pass filtered at 6 kHz, digitized at 20 kHz with a Digidata 1550A (Molecular Devices), and acquired and analyzed using pClamp 10.5 programs (Clampfit, Molecular Devices). Cells were voltage-clamped at −65 mV for recordings of excitatory postsynaptic currents (EPSCs; ChR2 = 10 cells from 5 rats, NpHR = 8 cells from 5 rats) or 0 mV for recordings of inhibitory postsynaptic currents (IPSCs; ChR2 = 5 cells from 3 rats) for 5 − 10 min to allow equilibration of pipette and intercellular solutions prior to data collection. Recordings were made from one cell in a slice, so cell and slice numbers are equivalent. Optical stimulation of the dentate gyrus was performed using 488 nm light for ChR2 stimulation and 593 nm light for NpHR stimulation. Three stimulation durations were used to test activation of the opsins (16 ms, 50 ms, and 500 ms). Following recording of responses to optical activation, either tetrodotoxin (TTX; 2 µM; Tocris Bioscience; Minneapolis, MN) to block action potentials, kynurenic acid (1 mM; Sigma Aldrich; St. Louis, MO) to block EPSCs, or bicuculline methiodide (30 µM; Tocris Bioscience; Minneapolis, MN) to block IPSCs was added to the circulating ACSF.

2.7. Analysis of 7SComplex

7S Complex was measured from synaptosomal extracts as previously described in detail (Matveeva et al., 2007, 2012a; Matveeva et al., 2012b, 2008; Matveeva et al., 2003).

2.8. Statistical analysis

2.8.1. Electrophysiology data analysis

Electrophysiology data analysis was performed using Graphpad Prism software (Graphpad Software; La Jolla, CA), using one-way ANOVA followed by Tukey's post hoc tests. Unless otherwise indicated, data are expressed as mean ± SEM, and significance was set at $p < 0.05$.

2.8.2. Microelectrode array analysis

Raw amperometric glutamate release data and event markers were analyzed using custom exported MatLab-based software, to determine maximum amplitude, exponential rate of signal decay (k-1), uptake rate (k-1*amp, glutamate only), peak or trough area, rise/drop time (T_{rise}/drop), and time for 80 % of signal decay (T_{80}), as we have previously described (Ledo et al., 2017; Stephens et al., 2011, 2014). Grouped results of single comparisons of these metrics were tested for normality with the Shapiro-Wilk normality test and analyzed using repeated measures analysis of variance (ANOVA with Bonferroni post-hoc) or a two-tailed Student's *t*-test when data were normally distributed. The Wilcoxon signed rank test for paired samples or the Mann-Whitney *U* test for unpaired samples was used when normally-distributed population responses could not be established.

3. Results

3.1. Distribution of opsins

Viral vector injections vary as to distribution of the targeted expression from the injection site. In this study we found that unilateral injection of ChR2 and NpHR not only resulted in expression within the ipsilateral dentate gyrus neurons but also spread to the contralateral hemisphere, likely from the commissural projections associated with hippocampal mossy cells and pyramidal neurons. Transfection of ChR2 resulted in widespread labeling of both principal cells and interneurons

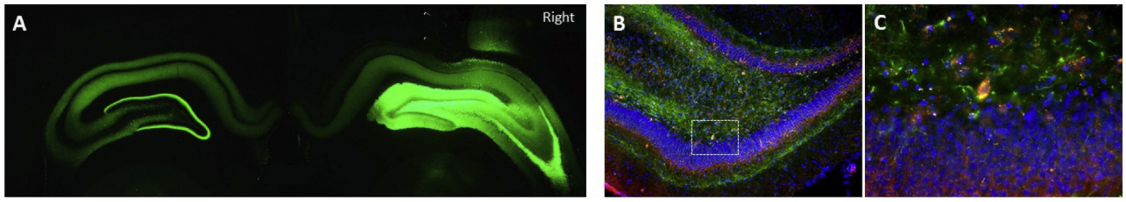

Fig. 2. Distribution of Transfected AAV Constructs. A. ChR2-YFP expression in DG (10X) showing bilateral distribution of AAV2/5 − CHR2-hSyn-EYFP in the hippocampus 6 weeks after a single injection (1 µl) into the right DG. B. AAV2/5-hSyn-NpHR 3.0-EYFP transfection (EYFP, green) and GAD67 immunolabeling (red) in the DG of a different rat (10X). There is a predominant colocalization of EYFP and GAD67 label, consistent with preferential transfection of GABAergic, inhibitory neurons. C. Enlargement of the boxed area in B, centered on a co-labeled hilar interneuron.

(Fig. 2). In addition, transfection of NpHR in the rat dentate gyrus resulted in co-immunolabeling primarily with GABAergic neurons, consistent with electrophysiological results (Fig. 2, also see Figs. 5, 6 and 7). We have evaluated the durability and longevity of both ChR2 and NpHR proteins. Electrophysiological responses to light stimulation in hippocampal slices (Figs. 4–6) remained robust for up to 15 weeks following viral inoculation, supported by continued demonstration of the GFP reporter protein out to 15 weeks. This range encompassed the duration of the experiments.

3.2. Light-induced glutamate release

Action potential generation in glutamatergic neurons results in the release of glutamate in the synaptic cleft between the pre- and post-synaptic neurons and spillover into the extracellular space, where it is largely inactivated by low affinity/high capacity uptake into glia. (Danbolt, 2001) In theory, when a large population of neurons fire synchronized action potentials, a large release of glutamate would be detected in the terminal region/extracellular space of that neuron population, but to date, very few studies have examined neurotransmitter release combined with optical stimulation. In this study we attached an optical fiber (200 µm o.d. ~200 µm from the recording sites) to our ceramic-based Pt MEA, which was configured to directly record tonic and phasic glutamate release (Burmeister et al., 2002), and lowered the assembly into the DG.

Fig. 3 shows precise optical control of glutamate release using variable light intensities (0.2 mW–50 mW). There was clear indication that the amplitude of the glutamate release was dependently related to power and the duration of the light emission. Repeated stimulation at 1 min intervals were extremely reproducible and did not show signs of tachyphylaxis. Furthermore, at equivalent power delivered at the tip of the fiber optic cannula (~4 to 5 mW), we did not observe significant differences in the amount of glutamate release whether using a light pulse train (20 ms, 40 Hz, for 2.5 s) or constant light activation (~2.5 s). We observed a maximal signal plateau at around 50 mW (data not shown). Based on our previous experience with evoked release of glutamate this was likely due to two major factors: 1) the density of synapses proximal to the MEA and 2) the maximal amount of light dispersion in the brain, which for blue light (488 nm) is estimated at no more than 1 mm (Bernstein et al., 2008; Yizhar et al., 2011). Furthermore, the temporal dynamics of glutamate release produced by ChR2 activation were similar to what we have previously reported using other forms of stimulation (high potassium, drug induced or behavior) (Stephens et al., 2014; Hunsberger et al., 2015; Miller et al., 2015; Quintero et al., 2007; Thomas et al., 2012). The dose-response of the glutamate signals vs. light power seen from light activation had a wider dynamic range and precision than we have seen from other methods involving micropipette drug applications, electrical stimulation or behavioral activation (Burmeister et al., 2002; Hascup et al., 2010; Onifer et al., 2012). These results support the hypothesis that the ChR2-control of glutamate release was robust and precisely regulated by the light stimulus.

3.3. Electrophysiological outcomes of ChR2 and NpHR activity in dentate gyrus granule cells (DGCs)

Transfection of ChR2 in rat dentate gyrus resulted in prominent labeling of principal, presumably glutamatergic neurons as well as presumptive GABAergic interneurons. Transfection of NpHR in the rat dentate gyrus resulted in prominent co-immunolabeling with GABAergic neurons (Fig. 2B, C); hilar mossy cells were also likely transfected. The functional outcomes of optical stimulation are important to our understanding of how these neurons affect the dentate gyrus circuit. For this study, we used optical stimulation while recording from DGCs to assess the functional outcomes of transfection of these channels into the dentate gyrus of the hippocampus. Stimulation in slices from rats transfected with AAV2/5-Syn-ChR2-EYFP resulted in direct inward currents in the recorded DGCs, which exhibited an

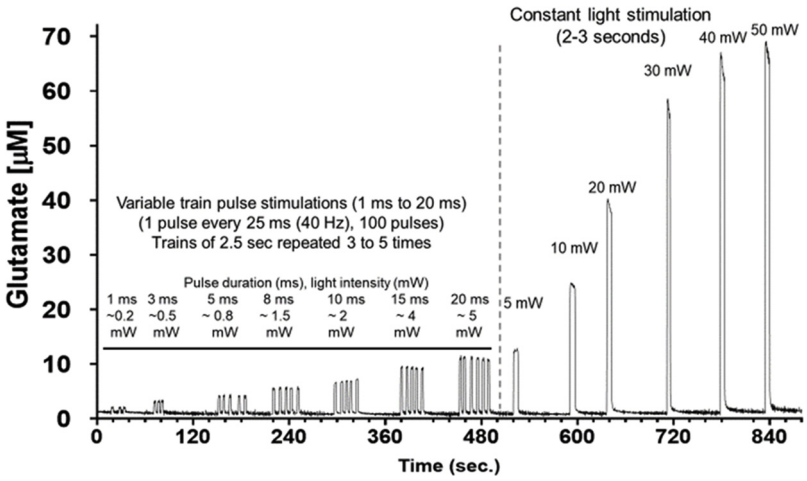

Fig. 3. Light intensity dependent increases in glutamate release. Blue laser-induced release of glutamate in rat DG using MEA + waveguide array. Comparison of pulse trains (100 pulses) with variable pulse durations vs. constant blue laser activations. A range of 0.2 − 50 mW laser intensities were used to produce reproducible light intensity-dependent, increases in extracellular glutamate.

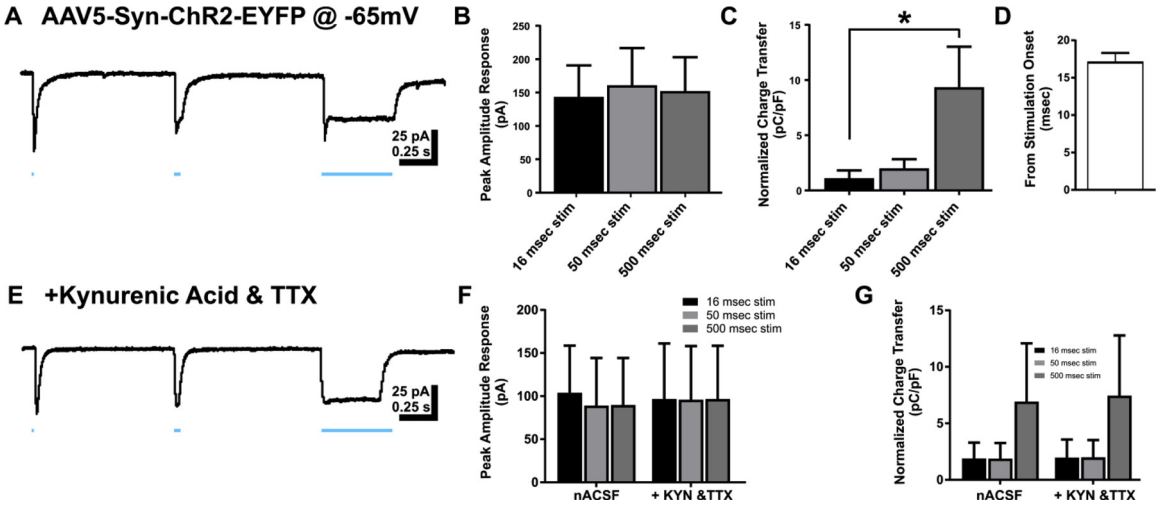

Fig. 4. Channelrhodopsin (ChR2)-activated inward currents in dentate granule cells. A. Representative recording of response in dentate granule cell (DGC) held at −65 mV to blue light in rat transfected with ChR2. B. Bar graph of peak amplitude of responses to ChR2 activity at 3 stimulation durations 16 msec, 50 msec, and 500 msec. C. Bar graph of charge transfer normalized to whole cell capacitance measures for direct ChR2 activity at 16 msec, 50 msec, and 500 msec durations. D. Bar graph of latency to peak response following blue light onset. E. Representative trace of recorded DGC response to blue light in the presence of kynurenic acid and tetrodotoxin in circulating ACSF. F. Bar graph of peak amplitude responses of DGCs in nACSF and ACSF with kynurenic acid and tetrodotoxin added. G. Bar graph of charge transfer normalized to whole cell capacitance in DGCs recorded in nACSF and ACSF with kynurenic acid and tetrodotoxin added. Data represented as mean ± SEM. * $p < 0.05$.

increase in charge transfer during 16 msec to 500 msec stimulation, with no stimulus time-related differences in peak amplitude (peak amplitude 16 ms stim = 143.73 ± 46.99 pA, peak amplitude 50 ms stim = 160.62 ± 55.54 pA, peak amplitude 500 ms stim = 152.37 ± 50.70 pA; one-way ANOVA, $F(2,27) = 0.03$, $p = 0.97$. In contrast, since responses were sustained during the light stimulus, the electrical charge over time (i.e., the charge transfer) dramatically increased as pulse width increased. This increase in charge transfer reached statistical significance during a comparison of the 16 msec and 500 msec pulse widths (charge transfer 16 msec stim = 1.12 ± 0.71 pC/pF, charge transfer 50 msec stim = 2.00 ± 0.82 pC/pF, charge transfer 500 msec stim = 9.35 ± 3.67 pC/pF; one-way ANOVA, $F(2,27) = 4.18$, $p = 0.03$; Tukey's post-hoc: $p = 0.96$, 16 msec stim vs 50 msec stim, $p = 0.04$, 16 msec stim vs 500 msec stim, $p = 0.07$ 50 msec stim vs 500 msec stim; $n = 10$ cells; Fig. 4 A–C). Together, the relatively short latency to response, similarity of peak amplitudes, and increased charge transfer with longer pulses suggest a direct activation of the recorded DGC, as opposed to a synaptic response (response latency = 17.17 ± 1.28 msec; Fig. 4D).

These findings prompted further assessment of direct versus synaptic responses by examining the sensitivity of the response to pharmacological blockade of synaptic receptors or sodium channels that are required for action potential-dependent neurotransmitter release. The large inward currents observed during activation of ChR2 were insensitive to both kynurenic acid and TTX in recorded DGCs (peak amplitude 16 ms stim = 96.82 ± 64.21 pA, peak amplitude 50 ms stim = 95.86 ± 62.23 pA, peak amplitude 500 ms stim = 96.79 ± 61.62 pA; charge transfer 16 msec stim = 2.43 ± 1.76 pC/pF, charge transfer 50 msec stim = 2.41 ± 1.70 pC/pF, charge transfer 500 msec stim = 8.70 ± 5.97 pC/pF; Two-way ANOVA, $F(2,12) = 0.2821$, $p = 0.76$; $n = 5$ cells; Fig. 4E–G), suggesting these currents were generated directly within the recorded granule cell, consistent with ChR2 expression in transfected DGCs. Small, transient inward currents (superimposed on the initial portion of the evoked inward currents) were sensitive to kynurenic acid or TTX, consistent with a separate glutamate receptor-mediated synaptic component in some neurons.

A subset of DGCs in ChR2 transfected animals were recorded while voltage-clamped at 0 mV to isolate putative $GABA_A$ receptor-mediated inhibitory responses. Optical stimulation of ChR2 resulted in transient, large outward currents with no significant difference in peak amplitude between stimulation durations (peak amplitude: 16 msec stim = 244.63 ± 109.29 pA; 50 msec stim = 246.73 ± 110.03 pA; 500 msec = 253.70 ± 112.08 pA; $F(2,12) = 0.001$, $p = 0.99$; $n = 5$ cells; Fig. 5 A, B). Peak amplitude of the outward current was therefore not directly related to stimulus duration. Unlike the inward currents evoked at −65 mV, the increase in light stimulation pulse width did not

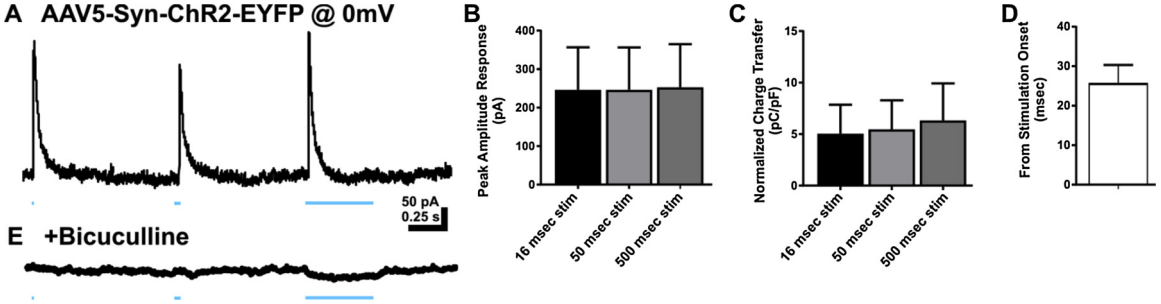

Fig. 5. ChR2 stimulation elicited $GABA_A$ receptor-mediated inhibitory synaptic responses in DGCs. A. Representative trace of response in DGC held at 0 mV to blue light in rat transfected with ChR2. B. Bar graph of peak amplitude of responses to ChR2 activity at 3 stimulation durations 16 msec, 50 msec, and 500 msec. C. Bar graph of charge transfer normalized to whole cell capacitance measures for direct ChR2 activity at 16 msec, 50 msec, and 500 msec durations. D. Bar graph of latency to peak response following blue light onset. E. Representative trace demonstrating sensitivity of responses to bicuculline (30 μM). Data represented as mean ± SEM.

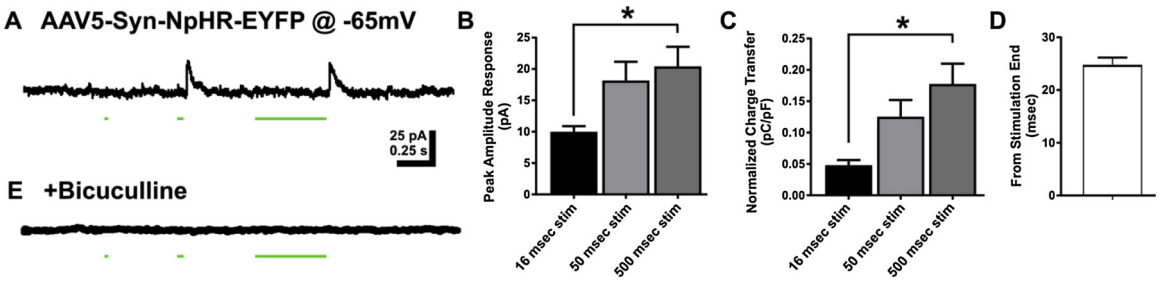

Fig. 6. DGC responses to activation of halorhodopsin (NpHR). A. Representative trace of response in DGC held at −65 mV to blue light activity in rat injected with NpHR. Outward currents developed at the offset of the inhibitory stimulus. B. Bar graph of peak amplitude of responses to NpHR activity at 3 stimulation durations 16 msec, 50 msec, and 500 msec. C. Bar graph of charge transfer normalized to whole cell capacitance measures for direct ChR2 activity at 16 msec, 50 msec, and 500 msec durations. D. Bar graph of latency to peak response following blue light offset. E. Representative trace demonstrating sensitivity of responses to bicuculline. Data represented as mean ± SEM. * $p < 0.05$.

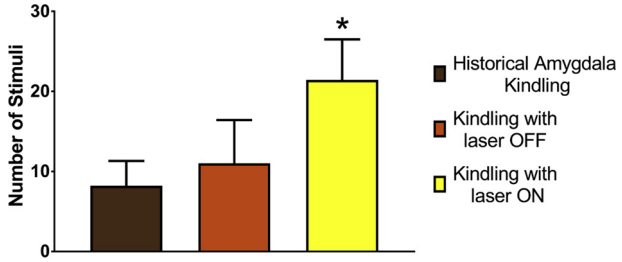

Fig. 7. Mitigation of epileptogenesis by expression and activation of halorhodopsin (NpHR). NpHR animals receiving overlapping yellow light activation (2−3 s) during 1-sec electrical stimulation of amygdala (yellow bar) required more stimuli ($P < 0.03$) to achieve stage 4/5 seizures (21.4 ± 5.1 [SD]; n = 5) than those without light activation (green bar; 11.0 ± 5.4; n = 4) or historical non-transfected controls (Matveeva et al., 2007, 2012a; Matveeva et al., 2008, 2003) (brown bar; 8.2 ± 3.1).

result in increased outward current charge transfer in recorded DGCs (charge transfer 16 msec stim = 5.04 ± 2.81 pC/pF; 50 msec stim = 5.47 ± 2.81 pC/pF; 500 msec stim = 6.33 ± 3.61 pC/pF; one-way ANOVA, F(2,12) = 0.04, p = 0.96). The response latency was longer than for excitatory events evoked by optical stimulation of ChR2 (response latency = 25.83 ± 4.50 msec; unpaired *t*-test (13) = 2.482, p = 0.02; Fig. 5D). Evoked outward currents were sensitive to bicuculline (Fig. 5E), indicating they were mediated by $GABA_A$ receptor activation. This suggests that ChR2 transfection also occurred in inhibitory neurons that project to DGCs, and/or in hilar mossy cells that mediate feedforward, di-synaptic inhibition of DGCs, in addition to the glutamatergic DGCs themselves.

Optical activation of AAV2/5-Syn-NpHR-EYFP, however, resulted in GABAergic inhibition of DGCs, and no direct inhibition of the DGC membrane was detected. The outward currents generated after activation of NpHR exhibited increased amplitude as stimulus duration increased from 16 to 500 msec (peak amplitude 16 msec stim = 9.98 ± 0.91 pA; 50 msec stim = 18.19 ± 2.98pA; 500 msec stim = 20.42 ± 3.13 pA; one-way ANOVA, F(2,21) = 4.64, p = 0.02; Tukey's post hoc: p = 0.08 16 msec stim vs 50 msec stim, p = 0.02 16 msec stim vs 500 msec stim, p = 0.81 50 msec stim vs 500 msec stim; n = 8 cells; Fig. 6 A,B). Similarly, charge transfer also increased with longer stimulus pulse widths (charge transfer 16 msec stim = 0.05 ± 0.01 pC/pF; 50 msec stim = 0.13 ± 0.03 pC/pF; 500 msec stim = 0.18 ± 0.03 pC/pF; one-way ANOVA, F(2,21) = 7.34, p = 0.004; Tukey's post hoc: p = 0.07, 16 msec stim vs 50 msec stim; p = 0.003, 16 msec stim vs 500 msec stim; p = 0.30, 50 msec stim vs 500 msec stim; Fig. 6C). Rather than being evoked at the onset of the stimulus, outward currents evoked by activating NpHR developed immediately after the light stimulus offset. The latency from the light stimulus offset to outward current onset was similar to that for synaptic responses evoked after activation of inhibitory neurons by ChR2 (onset latency = 24.81 ± 1.36 msec, Fig. 6D). This suggested they resulted from the removal of the inhibitory NpHR stimulus. The light-evoked outward currents were also sensitive to bicuculline (Fig. 6E), indicating they were mediated by $GABA_A$ receptors and consistent with rebound from NpHR-mediated inhibition of local inhibitory GABA neurons that projected to the recorded DGCs. These data are consistent with immunolabeling, which demonstrated a predominant NpHR transfection into GABAergic neurons (Fig. 2).

3.4. Behavioral responses to ChR2- and NpHR-optogenetic stimulation

Five rats were transfected with ChR2 injected into DG. After 6 weeks, they received twice-daily stimuli with 50 mW blue light. Two developed Racine Stage 1 seizures with seven stimuli before pulling off their MEA pedestals. One rat progressed to Stage 2 after 27 stimuli and one to Stage 3 after 15 stimuli. Finally, one rat had two consecutive Stage 5 seizures with the 18th and 19th stimuli. Stimulus-induced release of neurotransmitter from synaptic vesicles is facilitated by docking to and fusion of the vesicle membrane with the presynaptic plasma membrane, mediated by integral membrane proteins called SNAREs. In neurons, the 7S SNARE complex (7SC) is minimally required for vesicle/plasma membrane fusion (Weber et al., 1998); formation of stable 7SC is believed to represent one of the last steps before membrane fusion and is thus a hallmark of synaptic vesicles that are in a "ready-release" state. The 7SC hippocampal ipsilateral/contralateral ratio of the rat that experienced two consecutive Stage 5 seizures was 1.28, consistent with enhanced stimulus-induced synaptic transmission and consistent with our studies of fully electrically kindled rats stimulated from diverse sites (Matveeva et al., 2007, 2012a; Matveeva et al., 2012b, 2008; Matveeva et al., 2003).

We also evaluated the effect of yellow light stimulation of NpHR to supress epileptogenesis in the kindling model (Fig. 7). Nine rats were DG-transfected with NpHR. After 5 weeks, rats were implanted with kindling electrodes into right basal amygdala and a guide cannula for the fiber optic cable into right DG. One week later, rats (n = 5) were then stimulated twice/day: yellow light was applied for 2−3 sec followed immediately by a 1 s kindling stimulation at the predetermined after-discharge threshold, such that laser stimulation temporally overlapped kindling stimulation. Controls (n = 4) received only the 1 s kindling stimulation twice/day. Optogenetically inhibited rats required more stimuli to achieve stage 4/5 seizures than controls ($p < 0.03$) or historical controls from our laboratory (Matveeva et al., 2007, 2012a; Matveeva et al., 2008) and the literature (Le and La Salle, 1981).

4. Discussion

We aimed to determine how optogenetically-mediated neural network changes promote or inhibit hippocampal epileptic network activity and epileptogenesis. Although this study did not aim to determine

specific component mechanisms at hierarchies below the network level, results provide important information on how the evolution of a pathologic network can be enhanced or impeded by altering neuronal activity. Further, studies directed at the hierarchical level of network interactions may augment interpretation of outcomes from reductionist studies that are typically used to identify specific anatomic, molecular, or genetic mechanisms. Notably, hierarchical relationships are not necessarily linear and therefore prediction of network or system behavior as a function of changes in cell-type specific activity is inherently uncertain, and understanding epileptogenic network activity is therefore informative for understanding effects of cell-type specific pathologies. It is also important in the context of developing translationally relevant therapies for complex, multi-hierarchical disorders like epilepsy that involve cellular, network, and system pathologies.

Serotype-specific adeno-associated viruses (AAV) can be used to transfect cells in vivo via stereotaxic injection. Selective neurotropism of specific AAV serotypes can help delimit transfection and choice of promoters can restrict expression of the opsin protein. Thus, this technique, utilizing a highly focal light stimulus to limit the area of activated opsins, allows for considerable cell type specificity with high temporal and spatial precision. The extent of viral spread and cell tropism can be quite different among serotypes, dependent on target tissue and species. We used a recombinant AAV2/5 serotype, that is, the vectors contain AAV2 terminal repeats flanking the opsin-recorder cassette under the control of the synuclein promoter in an AAV5 capsid. This serotype has been shown to transfect almost the entire rostral to caudal extent of the dorsal hippocampal formation, including the DG granule cell layer and neurons within the entire pyramidal layer in the CA1-CA3 region (Burger et al., 2004), consistent with our observations (Fig. 2). The AAV5 capsid, which binds sialic acid on the cell surface and uses platelet-derived growth factor (PDGFR) for entry (Di Pasquale et al., 2003; Walters et al., 2001), restricts recorder (GFP) expression to neurons when used with the SynI neuronal synapsin promoter (Kugler et al., 2003; Shevtsova et al., 2005). Data presented here indicate that AAV serotype 2/5 at the titer range we used transfects excitatory and inhibitory neurons in the hippocampal formation.

Several promoters have been intensively studied (Burger et al., 2004; Holehonnur et al., 2014; Watakabe et al., 2015). α-Calcium/calmodulin-dependent kinase II (αCamKII) and SynI are most commonly used for neuronal transfection. Both promoters differentially transfect multiple neuronal types: GFP reporter is seen in both parvalbumin-positive GABA neurons and in large excitatory pyramidal cells independent of several AAV serotypes and using either neuronal promoter, but the expression levels of the transduced neurons is variable Watakabe et al., 2015). Interestingly, Nathanson et al. reported that both SynI and αCamKII promoters in an AAV1 serotype demonstrated an excitatory/inhibitory preference that changed by titer of the viral solution. (Nathanson et al., 2009) Differential levels of expression in at least two neuronal types may explain the electrophysiological data we present here. In this regard, it is well recognized that relatively small numbers of hippocampal GABA neurons, as demonstrated in Fig. 2B and C, can drive an excitatory synchronous volley and inhibiting restricted numbers of GABA neurons can increase evoked seizure threshold and shorten seizure duration (Khoshkhoo et al., 2017; Smith, 2013; Yekhlef et al., 2015).

The apparent spread of virus we observed (Fig. 2) helps ensure a wide regional, if not homogenous, level of expression among neurons. The cell-preferring but not cell-specific neurotropism of our AAV2/5 serotype helps delimit transfection to neurons, and our choice of promoter restricts expression of the opsin protein but does not alter constitutive cellular function. Because of the apparent (and fortuitous) differential expression of these channels among cell types, this model system with a single transfection vector is uniquely positioned to amplify and perturb both excitatory and inhibitory circuits that participate in network changes associated with acquired epileptogenesis. These characteristics can be exploited to optogenetically induce (gain-of-function) or inhibit (loss-of-function) epileptogenesis and relate these effects to network change, and to specific behavioral, cellular, electrophysiological and molecular outcomes. This system is especially useful in isolating the role of network activity in epileptogenesis, as only those cells expressing the particular opsin exposed to the correct wavelength of light will respond. Other factors like cell death of vulnerable neuron populations or robust mossy fiber sprouting that are observed in animal models of epilepsy are less likely to occur in this system (Shibley and Smith, 2002; Winokur et al., 2004).

Electrical kindling paradigms using amygdala, perforant path, or hippocampus as the stimulation site all require considerably fewer stimuli to reach full kindling than we observed using our optogenetic technique (Matveeva et al., 2007). Stimulation sites external to and direct electrical stimulation of the dentate gyrus result in a large synchronous depolarization volley arising there and a presumed more rapid conversion to pathological epileptiform networks. We postulate that use of our technique results in a smaller initial region of synchronization, a longer interval to recruit additional neuronal populations, and a slower development of necessary network changes as observed in our behavioral study. Such slowed development is reminiscent of focal epileptogenesis that develops after stroke and other focal injuries (Hunt et al., 2013; Kelly et al., 2001). Optogenetic kindling may allow for more controlled study of cellular, electrophysiological, and network changes of epileptogenesis, analogous to optogenetics employed in studies of seizure initiation and maintenance (Khoshkhoo et al., 2017; Ye and Kaszuba, 2017).

Interestingly, not only did the transfection of the AAV2/5 viral vectors used in this study differ in neuron populations that were transfected, but also the functional outcome of these opsins was also distinct at the cellular and network levels. ChR2 transfection led predominantly to direct activation of the recorded DGCs that was largely unresponsive to kynurenic acid or TTX application; small, transient evoked inward currents superimposed on the principal response were sensitive to kynurenic acid and were therefore consistent with activation of excitatory synaptic terminals. This function is consistent with the ChR2 transfection of glutamatergic principal neurons and glutamatergic synaptic terminals on the recorded neurons. ChR2 transfection of local, GABAergic neurons was also evident, and bicuculline-sensitive IPSCs were evoked in DGCs, an effect that could be mediated by directly activating inhibitory interneurons or via a feedforward/feedback microcircuit. In contrast, the transfection of NpHR primarily co-labeled with GABAergic neurons, and the activation of this opsin resulted in a transient outward current at the conclusion of the light stimulus, which was blocked by addition of the $GABA_A$ receptor antagonist, bicuculline. The blockade of this response in the presence of bicuculline and latency of response after conclusion of the stimulus are both consistent with the targeting of this viral transfection to GABAergic neurons in the dentate gyrus. Responses were not tested in other principal cells of the hippocampus (e.g., CA1 or CA3 pyramidal cells), and it remains possible that other hippocampal cell types will express the opsin and contribute to the inhibitory effect on kindling of NpHR activation. Interestingly, in optogenetically-evoked neocortical seizures, inhibitory neurons are recruited prior to excitatory neurons at seizure onset, and optogenetic inhibition of GABA neuron subtypes can inhibit seizure initiation or duration, possibly via disinhibition of local GABA circuitry (Khoshkhoo et al., 2017). Further studies to identify transfection prevalence in subpopulations of hippocampal GABA neurons may be beneficial in the use of this opsin to study the process of acquired epileptogenesis, including after TBI, stroke, and CNS infection. The demonstrated feasibility of optogenetic stimulation to alter neuronal circuit and system function in vivo and ex vivo shows promise for modifying epileptogenesis, but specific neural circuit interactions should also be assessed in the context of these behavioral and neural network outcomes as studies and trials move forward.

To date, little work has been done using optogenetic techniques to study epileptogenesis and the associated network changes. Previous

work in optogenetic activation of brain regions has demonstrated the ability to evoke or suppress seizures or seizure-like activity (Armstrong et al., 2013; Krook-Magnuson et al., 2013; Paz et al., 2013; Sukhotinsky et al., 2013). However, this study is the first to use *in vivo* real time measurement of glutamate with MEAs to assess the outcome of optical stimulation in transfected rodents (Parrot et al., 2015). Detection of glutamate release that is sensitive to both stimulation frequency and duration demonstrates the ability of these opsins to respond to variable stimuli and potentials as an adaptable response, which in these studies was epileptogenesis or its hindrance.

In a review, Chow and Boyden proposed that optogenetics be used as a therapeutic intervention in conditions for which a clear benefit may be obtained from switching on or off specific cell types, and for which there is no better alternative. (Chow and Boyden, 2013) Examples included retinitis pigmentosa, epilepsy, and spinal cord injury. Optogenetic therapeutics currently require the delivery of genetic constructs by means of a viral vector and once inside the body, bacterial or algal opsins may need to be stably expressed for weeks, months or even years, and this could trigger an adaptive glial or immune response. That said gene therapy for Parkinson's disease using AAV vectors has been advancing for the last decade, with continued refinements as knowledge advances. A recent clinical trial reported no clinically meaningful adverse events attributable to intraputaminal AAV2-neurturin, indwelling for up to two years. (Olanow et al., 2015) Instrumentation such as Deep Brain Stimulation electrodes for Parkinson's disease, Essential Tremor and dystonias (FDA-approved since 1999) and Vagal Nerve Stimulation for epilepsy (FDA-approved in 2005) can be safely implanted and function for years. Preclinical studies using optogenetic approaches to develop new therapeutics to affect brain disorders are in process.

Optogenetic stimulation to drive behavioral alteration has been successfully implemented using in vivo electrophysiological monitoring methods. Using opsin-transfected hippocampal cells, Krook-Magnuson et al. have used a closed-loop system to record real-time epileptiform activity in hippocampus and stop spontaneous temporal lobe seizures by light stimulation (Krook-Magnuson et al., 2013). A similar closed-loop paradigm has been used by Paz et al. to optogenetically control thalamus and interrupt seizures after cortical injury. (Paz et al., 2013) However, to our knowledge few studies have been reported that connect optogenetic stimulation to neuronal activation by monitoring neurotransmitter concentrations. Microdialysis allows direct measurements of neurotransmitter output in response to optogenetic stimulation, but does not provide the necessary high spatial and temporal resolution required to study the rapid phasic activity of glutamate (or other neurotransmitter) release (Zant et al., 2016). In vivo amperometry using MEAs, however, does allow for quantification of extracellular neurotransmitter levels at the temporal and spatial resolution of electrophysiologic recordings. As shown here and elsewhere, this method allows for real-time measurement of both phasic and tonic glutamate release. (Matveeva et al., 2012a; Stephens et al., 2014; Batten et al., 2017; Viereckel et al., 2016) A real-time electrochemical recording device has been used to study optogenetically controlled dopamine release in PC12 cell cultures (Chiu et al., 2014) and striatum of anesthetized rat (Bass et al., 2010), and acetylcholine in rat basal forebrain (Gritton et al., 2016). The measurements of glutamate using optogenetics coupled to the MEA technology in this study are an extension of the recently reported studies by Viereckel and colleagues in the mouse globus pallidus. (Viereckel et al., 2018) Viereckel and coworkers used viral injection into the subthalamic nucleus to produce a selective expression of channelrhodopsin via glutamate fibers to the globus pallidus. Light activation of the globus pallidus adjacent to the MEA produced rapid and transient overflow of glutamate that was light intensity-dependent. (Viereckel et al., 2018) In the present studies, we used a different viral construct that targeted neurons into the dentate gyrus of the rat hippocampus to produce channelrhodopsin expression in the hippocampal trisynaptic pathway. Optical stimulation of ChR2 produced transient release of glutamate somewhat analogous to the work of Viereckel and coworkers. However, there were two major differences observed not withstanding we used a different viral construct with a synapsin promotor and a different viral serotype. First, our light-evoked signals were very reproducible and were different in signal shape. Secondly, in comparison to Viereckel et al., our laser light pulses did not produce any photovoltaic effect or artifacts when the recording assembly was tested in vitro and we observed visible artifacts in the hippocampus of treatment naïve rats only at light intensities < 10 mW. The artifact/photovoltaic effects were different in shape and time course from those described by Viereckel and coworkers and were easily removed using the self-referencing sentinel sites. Thus, no correction was needed for calculation of the glutamate concentrations as seen in Viereckel et al. (Viereckel et al., 2018) Some of these differences are likely due to the different viral constructs employed in the two different studies, the orientation of the MEA to the optical fiber and the different brain regions studied.

5. Conclusions

This study demonstrates the integration of transfected opsin channels into a rodent model with both in vivo and ex vivo functional outcome measures. Coupled with MEA real-time monitoring, these findings will provide a foundation for better understanding of how neuron population activity selectively contributes to disease progression and upon which future use of optogenetic interventions to modify neurological diseases, including epilepsy, can be based. Treatments affecting individual components of the disorder (e.g., GABA receptor modulators, sodium channel blockers) have failed to prevent epileptogenesis, even though clearly they can be effective against seizures. This proof of principle study indicates that modifying activity at the network level can modify aspects of the epileptogenic process. These findings may provide valuable insight for novel therapy development, and will inform future, more reductionist approaches aimed at functionally relevant aspects of the network-driven disease modification.

Financial interests

GAG is the Owner of Quanteon, LLC that manufactures and sells FAST MK III recording system used for measuring glutamate.

Acknowledgements

Supported by Veterans Administration Medical Center (SWW, JTS); DARPA N66001-09-C-2080 (GAG); NIH NS088608 (BNS).

References

Armstrong, C., Krook-Magnuson, E., Oijala, M., Soltesz, I., 2013. Closed-loop optogenetic intervention in mice. Nat. Protoc. 8, 1475–1493.
Bass, C.E., Grinevich, V.P., Vance, Z.B., Sullivan, R.P., Bonin, K.D., Budygin, E.A., 2010. Optogenetic control of striatal dopamine release in rats. J. Neurochem. 114, 1344–1352.
Batten, S.R., Matveeva, E.A., Whiteheart, S.W., Vanaman, T.C., Gerhardt, G.A., Slevin, J.T., 2017. Linking kindling to increased glutamate release in the dentate gyrus of the hippocampus through the STXBP5/tomosyn-1 gene. Brain Behav. 7, e00795.
Bernstein, J.G., Han, X., Henninger, M.A., et al., 2008. Prosthetic systems for therapeutic optical activation and silencing of genetically-targeted neurons. Proc. SPIE. Int. Soc. Opt. Eng. 6854 68540H.
Boychuk, J.A., Butler, C.R., Halmos, K.C., Smith, B.N., 2016. Enduring changes in tonic GABAA receptor signaling in dentate granule cells after controlled cortical impact brain injury in mice. Exp. Neurol. 277, 178–189.
Boyden, E.S., Zhang, F., Bamberg, E., Nagel, G., Deisseroth, K., 2005. Millisecond-timescale, genetically targeted optical control of neural activity. Nat. Neurosci. 8, 1263–1268.
Burger, C., Gorbatyuk, O.S., Velardo, M.J., et al., 2004. Recombinant AAV viral vectors pseudotyped with viral capsids from serotypes 1, 2, and 5 display differential efficiency and cell tropism after delivery to different regions of the central nervous system. Mol. Ther. 10, 302–317.
Burmeister, J.J., Gerhardt, G.A., 2001. Self-referencing ceramic-based multisite microelectrodes for the detection and elimination of interferences from the measurement of

L-glutamate and other analytes. Anal. Chem. 73, 1037–1042.
Burmeister, J.J., Davis, V.A., Quintero, J.E., Pomerleau, F., Huettl, P., Gerhardt, G.A., 2013. Glutaraldehyde cross-linked glutamate oxidase coated microelectrode arrays: selectivity and resting levels of glutamate in the CNS. ACS Chem. Neurosci. 4, 721–728.
Burmeister, J.J., Pomerleau, F., Palmer, M., Day, B.K., Huettl, P., Gerhardt, G.A., 2002. Improved ceramic-based multisite microelectrode for rapid measurements of L-glutamate in the CNS. J. Neurosci. Methods 119, 163–171.
Butler, C.R., Boychuk, J.A., Smith, B.N., 2015. Effects of rapamycin treatment on neurogenesis and synaptic reorganization in the Dentate Gyrus after controlled cortical impact injury in mice. Front. Syst. Neurosci. 9, 163.
Butler, C.R., Boychuk, J.A., Smith, B.N., 2016. Differential effects of rapamycin treatment on tonic and phasic GABAergic inhibition in dentate granule cells after focal brain injury in mice. Exp. Neurol. 280, 30–40.
Butler, C.R., Boychuk, J.A., Smith, B.N., 2017. Brain injury-induced synaptic reorganization in hilar inhibitory neurons is differentially suppressed by rapamycin. eNeuro 4.
Chiu, W.T., Lin, C.M., Tsai, T.C., et al., 2014. Real-time electrochemical recording of dopamine release under optogenetic stimulation. PLoS One 9, e89293.
Chow, B.Y., Boyden, E.S., 2013. Optogenetics and translational medicine. Sci. Transl. Med. 5 177ps175.
Danbolt, N.C., 2001. Glutamate uptake. Prog. Neurobiol. 65, 1–105.
Deisseroth, K., Etkin, A., Malenka, R.C., 2015. Optogenetics and the circuit dynamics of psychiatric disease. JAMA 313, 2019–2020.
Di Pasquale, G., Davidson, B.L., Stein, C.S., et al., 2003. Identification of PDGFR as a receptor for AAV-5 transduction. Nat. Med. 9, 1306–1312.
Govorunova, E.G., Sineshchekov, O.A., Janz, R., Liu, X., Spudich, J.L., 2015. NEUROSCIENCE. Natural light-gated anion channels: a family of microbial rhodopsins for advanced optogenetics. Science 349, 647–650.
Gritton, H.J., Howe, W.M., Mallory, C.S., Hetrick, V.L., Berke, J.D., Sarter, M., 2016. Cortical cholinergic signaling controls the detection of cues. Proc. Natl. Acad. Sci. U. S. A. 113, E1089–1097.
Hascup, E.R., Hascup, K.N., Stephens, M., et al., 2010. Rapid microelectrode measurements and the origin and regulation of extracellular glutamate in rat prefrontal cortex. J. Neurochem. 115, 1608–1620.
Holehonnur, R., Luong, J.A., Chaturvedi, D., et al., 2014. Adeno-associated viral serotypes produce differing titers and differentially transduce neurons within the rat basal and lateral amygdala. BMC Neurosci. 15, 28.
Hunsberger, H.C., Rudy, C.C., Batten, S.R., Gerhardt, G.A., Reed, M.N., 2015. P301L tau expression affects glutamate release and clearance in the hippocampal trisynaptic pathway. J. Neurochem. 132, 169–182.
Hunt, R.F., Boychuk, J.A., Smith, B.N., 2013. Neural circuit mechanisms of post-traumatic epilepsy. Front. Cell. Neurosci. 7, 89.
Kelly, K.M., Kharlamov, A., Hentosz, T.M., et al., 2001. Photothrombotic brain infarction results in seizure activity in aging Fischer 344 and Sprague Dawley rats. Epilepsy Res. 47, 189–203.
Khoshkhoo, S., Vogt, D., Sohal, V.S., 2017. Dynamic, cell-type-Specific roles for GABAergic interneurons in a mouse model of optogenetically inducible seizures. Neuron 93, 291–298.
Klein, P., Dingledine, R., Aronica, E., et al., 2018. Commonalities in epileptogenic processes from different acute brain insults: Do they translate? Epilepsia 59, 37–66.
Krook-Magnuson, E., Armstrong, C., Oijala, M., Soltesz, I., 2013. On-demand optogenetic control of spontaneous seizures in temporal lobe epilepsy. Nat. Commun. 4, 1376.
Kugler, S., Lingor, P., Scholl, U., Zolotukhin, S., Bahr, M., 2003. Differential transgene expression in brain cells in vivo and in vitro from AAV-2 vectors with small transcriptional control units. Virology 311, 89–95.
Le, Gal, La Salle, G., 1981. Amygdaloid kindling in the rat: regional differences and general properties. In: Wada, J.A. (Ed.), Kindling 2. Raven Press, New York, NY, pp. 31–47.
Ledo, A., Lourenco, C.F., Laranjinha, J., Brett, C.M., Gerhardt, G.A., Barbosa, R.M., 2017. Ceramic-based multisite platinum microelectrode arrays: morphological characteristics and electrochemical performance for extracellular oxygen measurements in brain tissue. Anal. Chem. 89, 1674–1683.
Matveeva, E.A., Vanaman, T.C., Whiteheart, S.W., Slevin, J.T., 2007. Asymmetric accumulation of hippocampal 7S SNARE complexes occurs regardless of kindling paradigm. Epilepsy Res. 73, 266–274.
Matveeva, E.A., Vanaman, T.C., Whiteheart, S.W., Slevin, J.T., 2008. Levetiracetam prevents kindling-induced asymmetric accumulation of hippocampal 7S SNARE complexes. Epilepsia 49, 1749–1758.
Matveeva, E.A., Whiteheart, S.W., Slevin, J.T., 2003. Accumulation of 7S SNARE complexes in hippocampal synaptosomes from chronically kindled rats. J. Neurochem. 84, 621–624.
Matveeva, E.A., Davis, V.A., Whiteheart, S.W., Vanaman, T.C., Gerhardt, G.A., Slevin, J.T., 2012a. Kindling-induced asymmetric accumulation of hippocampal 7S SNARE complexes correlates with enhanced glutamate release. Epilepsia 53, 157–167.
Matveeva, E.A., Price, D.A., Whiteheart, S.W., Vanaman, T.C., Gerhardt, G.A., Slevin, J.T., 2012b. Reduction of vesicle-associated membrane protein 2 expression leads to a kindling-resistant phenotype in a murine model of epilepsy. Neuroscience 202, 77–86.
Miller, E.M., Quintero, J.E., Pomerleau, F., Huettl, P., Gerhardt, G.A., Glaser, P.E., 2015. Simultaneous glutamate recordings in the frontal cortex network with multisite biomorphic microelectrodes: new tools for ADHD research. J. Neurosci. Methods 252, 75–79.
Nagel, G., Szellas, T., Huhn, W., et al., 2003. Channelrhodopsin-2, a directly light-gated cation-selective membrane channel. Proc. Natl. Acad. Sci. U. S. A. 100, 13940–13945.
Nathanson, J.L., Yanagawa, Y., Obata, K., Callaway, E.M., 2009. Preferential labeling of inhibitory and excitatory cortical neurons by endogenous tropism of adeno-associated virus and lentivirus vectors. Neuroscience 161, 441–450.
Olanow, C.W., Bartus, R.T., Baumann, T.L., et al., 2015. Gene delivery of neurturin to putamen and substantia nigra in Parkinson disease: a double-blind, randomized, controlled trial. Ann. Neurol. 78, 248–257.
Onifer, S.M., Quintero, J.E., Gerhardt, G.A., 2012. Cutaneous and electrically evoked glutamate signaling in the adult rat somatosensory system. J. Neurosci. Methods 208, 146–154.
Parrot, S., Denoroy, L., Renaud, B., Benetollo, C., 2015. Why optogenetics needs in vivo neurochemistry. ACS Chem. Neurosci. 6, 948–950.
Paxinos, G., Watson, C., 2005. The Rat Brain in Stereotaxic Coordinates, fifth edition. Academic Press, Inc., San Diego.
Paz, J.T., Davidson, T.J., Frechette, E.S., et al., 2013. Closed-loop optogenetic control of thalamus as a tool for interrupting seizures after cortical injury. Nat. Neurosci. 16, 64–70.
Quintero, J.E., Day, B.K., Zhang, Z., et al., 2007. Amperometric measures of age-related changes in glutamate regulation in the cortex of rhesus monkeys. Exp. Neurol. 208, 238–246.
Racine, R.J., 1972. Modification of seizure activity by electrical stimulation. II. Motor seizure. Electroencephalogr. Clin. Neurophysiol. 32, 281–294.
Shevtsova, Z., Malik, J.M., Michel, U., Bahr, M., Kugler, S., 2005. Promoters and serotypes: targeting of adeno-associated virus vectors for gene transfer in the rat central nervous system in vitro and in vivo. Exp. Physiol. 90, 53–59.
Shibley, H., Smith, B.N., 2002. Pilocarpine-induced status epilepticus results in mossy fiber sprouting and spontaneous seizures in C57BL/6 and CD-1 mice. Epilepsy Res. 49, 109–120.
Smith, B.N., 2013. "Maestro" Hub Neurons Orchestrate the Immature GABA Network Symphony. Epilepsy Curr. 13, 93–94.
Stephens, M.L., Quintero, J.E., Pomerleau, F., Huettl, P., Gerhardt, G.A., 2011. Age-related changes in glutamate release in the CA3 and dentate gyrus of the rat hippocampus. Neurobiol. Aging 32, 811–820.
Stephens, M.L., Williamson, A., Deel, M.E., et al., 2014. Tonic glutamate in CA1 of aging rats correlates with phasic glutamate dysregulation during seizure. Epilepsia 55, 1817–1825.
Sukhotinsky, I., Chan, A.M., Ahmed, O.J., et al., 2013. Optogenetic delay of status epilepticus onset in an in vivo rodent epilepsy model. PLoS One 8 (e6), 2013.
Thomas, T.C., Hinzman, J.M., Gerhardt, G.A., Lifshitz, J., 2012. Hypersensitive glutamate signaling correlates with the development of late-onset behavioral morbidity in diffuse brain-injured circuitry. J. Neurotrauma 29, 187–200.
Ulusoy, A., Sahin, G., Bjorklund, T., Aebischer, P., Kirik, D., 2009. Dose optimization for long-term rAAV-mediated RNA interference in the nigrostriatal projection neurons. Mol. Ther. 17, 1574–1584.
Viereckel, T., Dumas, S., Smith-Anttila, C.J., et al., 2016. Midbrain gene screening identifies a new mesoaccumbal glutamatergic pathway and a marker for dopamine cells neuroprotected in parkinson's disease. Sci. Rep. 6, 35203.
Viereckel, T., Konradsson-Geuken, A., Wallen-Mackenzie, A., 2018. Validated multi-step approach for in vivo recording and analysis of optogenetically evoked glutamate in the mouse globus pallidus. J. Neurochem. 145, 125–138.
Walters, R.W., Yi, S.M., Keshavjee, S., et al., 2001. Binding of adeno-associated virus type 5 to 2,3-linked sialic acid is required for gene transfer. J. Biol. Chem. 276, 20610–20616.
Watakabe, A., Ohtsuka, M., Kinoshita, M., et al., 2015. Comparative analyses of adeno-associated viral vector serotypes 1, 2, 5, 8 and 9 in marmoset, mouse and macaque cerebral cortex. Neurosci. Res. 93, 144–157.
Weber, T., Zemelman, B.V., McNew, J.A., et al., 1998. SNAREpins: minimal machinery for membrane fusion. Cell 92, 759–772.
Winokur, R.S., Kubal, T., Liu, D., Davis, S.F., Smith, B.N., 2004. Recurrent excitation in the dentate gyrus of a murine model of temporal lobe epilepsy. Epilepsy Res. 58, 93–105.
Ye, H., Kaszuba, S., 2017. Inhibitory or excitatory? Optogenetic interrogation of the functional roles of GABAergic interneurons in epileptogenesis. J. Biomed. Sci. 24, 93.
Yekhlef, L., Breschi, G.L., Lagostena, L., Russo, G., Taverna, S., 2015. Selective activation of parvalbumin- or somatostatin-expressing interneurons triggers epileptic seizure-like activity in mouse medial entorhinal cortex. J. Neurophysiol. 113, 1616–1630.
Yizhar, O., Fenno, L.E., Davidson, T.J., Mogri, M., Deisseroth, K., 2011. Optogenetics in neural systems. Neuron 71, 9–34.
Zant, J.C., Kim, T., Prokai, L., et al., 2016. Cholinergic neurons in the basal forebrain promote wakefulness by actions on neighboring non-cholinergic neurons: an opto-dialysis study. J. Neurosci. 36, 2057–2067.
Zhang, F., Gradinaru, V., Adamantidis, A.R., et al., 2010. Optogenetic interrogation of neural circuits: technology for probing mammalian brain structures. Nat. Protoc. 5, 439–456.